Quasi-TM Transmission Line Parameters of Coupled Lossy Lines Based on the Dirichlet to Neumann Boundary Operator

Thomas Demeester and Daniël De Zutter, *Fellow, IEEE*

***Abstract*—This paper presents a new multiconductor transmission line model for general 2-D lossy configurations based on mode reciprocity. Particular attention is devoted to elucidate the validity of the quasi-TM model and the approximations that have to be invoked to obtain this model. A new derivation of the complex capacitance matrix is given, especially taking into account the presence of semiconductors. This derivation automatically leads to a nonclassical circuit signal current definition and demands for a formulation of the complex inductance problem consistent with that definition. The relevant resistance, inductance, conductance, and capacitance circuit matrices are obtained by solving boundary integral equations only, making use of the Dirichlet to Neumann boundary operator for the different materials. This allows to simulate complex metal–insulator–semiconductor structures, as shown in the numerical examples.**

***Index Terms*—Conductor losses, multiconductor transmission line (MTL) model, quasi-TM approximation, substrate losses.**

I. Introduction

Due to the increase in operating frequencies, signal integrity issues become more and more critical, not only on the package and board levels, but also at the chip level. Today, very large scale integration (VLSI) circuit lumped resistance–capacitance (*RC*) models no longer suffice for adequate signal analysis, but are replaced by transmission line models. In the past, much attention has been paid to the analysis of metal–insulator–semiconductor (MIS) transmission lines. A very good overview of this work is given in the introduction of [1] and will not be repeated here. Using a variety of numerical techniques, these papers analyze the fundamental mode behavior as a function of frequency and semiconductor resistivity, revealing the existence of dielectric, slow-wave, and skin-effect modes. Additional data based on quasi-analytical approaches and measurements can, for example, be found in [2]–[4]. It is interesting to draw the attention to a series of papers dealing with semiconductor substrate noise coupling (see [5] and references therein). These papers use and/or discuss the validity of electroquasi-static *RC* modeling to predict noise coupling, and in this way also deal with the question of approximating the full Maxwell equations in the presence of semiconductors. Furthermore, an efficient quasi-TEM analysis for lossy lines, using a finite-element approach and its full-wave extension to semiconductor traveling-wave devices, including self-consistent carrier transport, have been presented in [6] and [7].

In [1], the quasi-TM model proposed in [8] is extended to include nonperfectly conducting metallic conductors. As shown, for example, in [9] and [10], these conductor losses can become dominant for narrow strip configurations. The transmission line model developed in [1] is obtained by carefully defining the meaning of voltage and current, remaining compatible with the complex power concept [11], [12]. To obtain the per unit length (p.u.l) complex capacitance and inductance, the quasi-static electric potential and the longitudinal current density are determined numerically using a combination of the method of lines (MoL) and the method of moments (MoM).

In this paper, the quasi-TM analysis of [1] is extended to the multiconductor case. Section II discusses the general geometry of the considered problem together with the relevant field equations. Contrary to what one might expect, the multiconductor case does not turn out to be a straightforward extension of the single line case. Section III shows that a coupled transmission line model with each modal voltage–current $(\mathbf{v}, \mathbf{i})$ solution corresponding to a modal field $(\mathbf{e}, \mathbf{h})$ solution must be based on mode orthogonality properties. Hence, the power orthogonality definition used in [1] must be replaced by a reciprocity based approach [13], as modal fields are not power orthogonal in the presence of lossy media. It must be noted that the approach in [11] is not the only one to enforce reciprocity. As originally presented in [14] and later extended to more complex configurations in [15] and [16], one can also choose to enforce power conservation for each mode separately, whereby modal reciprocity is still invoked to ensure the reciprocity of the resulting circuit model. Section IV-A presents the theoretical analysis leading to the definition of the capacitance matrix and to the meaning of voltages and currents. A lot of attention is devoted to clarify the various approximations that must be invoked to come to a quasi-TM analysis and to show under which conditions this quasi-TM analysis remains valid. Similar to the single line case, it turns out that the meaning of current must be interpreted with due care. To define the complex capacitance matrix, mode orthogonality, and hence, reciprocity, must again be invoked. Section IV-B is devoted to the numerical solution of the capacitance problem. For this numerical solution, the contrast current and the corresponding contrast surface charges are introduced. These charges and the corresponding potential distribution in the cross section are then determined by solving an appropriate boundary integral equation with the MoM. To solve this integral equation, a relationship between the normal

Manuscript received January 24, 2008; revised April 7, 2008. First published June 6, 2008; last published July 9, 2008 (projected).

The authors are with the Department of Information Technology, Ghent University, B-9000 Ghent, Belgium (e-mail: thomas.demeester@intec.ugent.be; daniel.dezutter@ugent.be).

Digital Object Identifier 10.1109/TMTT.2008.925215

0018-9480/$25.00 © 2008 IEEE

Authorized licensed use limited to: AT & T. Downloaded on May 13, 2009 at 10:24 from IEEE Xplore. Restrictions apply.

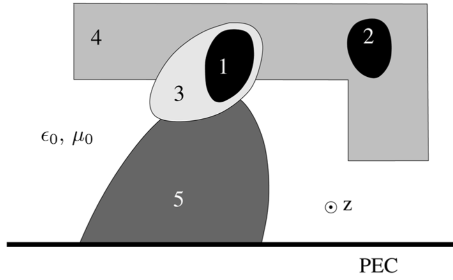

Fig. 1. General 2-D cross section to be considered. 1, 2: signal conductors ($\sigma \gg \omega\epsilon$), 3: lossless dielectrics (ϵ), 4: lossy dielectrics ($\sigma \ll \omega\epsilon$), 5: semiconductors ($\sigma$, ϵ).

derivative of the potential and the potential itself at the boundary of the different media is needed. This relationship is obtained by extending the surface admittance approach of [17], based on the Dirichlet to Neumann boundary operator, to the electro-quasi-static case. Section V discusses the inductance problem. Starting from the longitudinal component of the contrast current, is it shown that the longitudinal currents and the complex inductance matrix elements can also be determined by solving a boundary integral equation essentially using the differential surface admittance approach of [17] (again taking advantage of the Dirichlet to Neumann boundary operator). To correctly describe the problem in the presence of semiconductors, the theory of [17] and [18] has been reformulated as to carefully include the wave behavior in the longitudinal direction and the nonconstant potential in the cross section. The potential obtained from the capacitance problem remains necessary to solve the inductance problem. In contrast to the approach in [1], using a combination of the MoM and the MoL, the inductance problem is solved by using a surface integral equation only. The major advantage of such an approach, as opposed to volume discretization methods, is the considerably reduced number of unknowns when simulating large configurations (such as, for example, the last example presented in Section VI). Especially for the simulation of strong skin-effect behavior, boundary element methods tend to have a lower computational cost. However, as soon as more complicated semiconductor models are used, as in [7], volume discretization methods are indispensable. Section VI discusses a series of numerical examples, including some single-conductor reference examples and the full modal analysis of an on-chip interconnect structure with four coupled signal pairs. Finally, Section VII provides some conclusions.

II. Geometry of the Problem and Field Equations

Fig. 1 shows the general cross section of the considered multiconductor transmission line (MTL). It consists of piecewise homogeneous, nonmagnetic materials embedded in a lossless homogeneous background medium. In Fig. 1 a single perfectly electric conducting (PEC) ground plane is also shown, but its presence is not mandatory. In the sequel, a distinction is made between three types of materials: signal conductors such as 1 and 2 in Fig. 1, for which $\sigma \gg \omega\epsilon$ over the considered frequency range (for a PEC $\sigma \longrightarrow \infty$), lossless or lossy dielectrics such as 3 and 4 in Fig. 1, for which $\sigma = 0$ or $\sigma \ll \omega\epsilon$, and semiconductors such as 5. For simplicity, the homogeneous background medium is taken to be free space (ϵ_0, μ_0), but the analysis remains valid for any other dielectric background medium. A $e^{j\omega t}$ time dependence is assumed. The total number of signal conductors is N. Maxwell's curl equations can be cast into the following form:

$$\nabla_t e_z - \frac{\partial \mathbf{e}_t}{\partial z} = -j\omega\mu_0(\mathbf{u}_z \times \mathbf{h}_t) \tag{1}$$

$$\nabla_t \times \mathbf{e}_t = -j\omega\mu_0 h_z \mathbf{u}_z \tag{2}$$

$$\nabla_t h_z - \frac{\partial \mathbf{h}_t}{\partial z} = (\sigma + j\omega\epsilon)(\mathbf{u}_z \times \mathbf{e}_t) \tag{3}$$

$$\nabla_t \times \mathbf{h}_t = (\sigma + j\omega\epsilon) e_z \mathbf{u}_z \tag{4}$$

where the index t denotes the transversal (x, y) components. In the sequel, we will also use the divergence equation

$$\nabla_t \cdot \mathbf{e}_t + \frac{\partial e_z}{\partial z} = 0. \tag{5}$$

We want to obtain a transmission line model for the fundamental modes propagating along the z-axis. The number of fundamental modes N is equal to the number of signal conductors (i.e., two in the case of Fig. 1). The z dependence of mode $m(m = 1, 2, \ldots, N)$ is given by $e^{-j\beta_m z}$. In the absence of a PEC reference conductor, one of the conductors must be chosen as the reference conductor, and in that case, only $N - 1$ fundamental modes are needed. In the most general case, a full-wave analysis is needed to determine the modal wavenumbers β_m and the corresponding modal field distributions. In this paper, a quasi-TM approximation is proposed, based on the assumption that even at the highest frequency of interest, no wave phenomena occur in the transverse plane. This implies that the wavelength $\lambda_m = 2\pi/\text{Re}\,(\beta_m)$ of each propagating mode remains significantly larger than the relevant diameter of the cross section. Restricting ourselves to the fundamental modes, any solution of (1)–(4) for the transversal fields can be expressed as a superposition of these modes as [12]

$$\mathbf{e}_t(\boldsymbol{r}, z) = \sum_{m=1}^{N} \mathbf{E}_{\text{tm}}(\boldsymbol{r}) \left(K_m^+ e^{-j\beta_m z} + K_m^- e^{j\beta_m z}\right) \tag{6}$$

$$\mathbf{h}_t(\boldsymbol{r}, z) = \sum_{m=1}^{N} \mathbf{H}_{\text{tm}}(\boldsymbol{r}) \left(K_m^+ e^{-j\beta_m z} - K_m^- e^{j\beta_m z}\right). \tag{7}$$

$\mathbf{E}_{\text{tm}}$ and $\mathbf{H}_{\text{tm}}$ are the transversal modal field patterns, K_m^+ and K_m^- are the complex amplitudes of the modes, respectively, propagating in the positive and negative z-direction and $\boldsymbol{r} = x\mathbf{u}_x + y\mathbf{u}_y$.

III. Coupled Transmission Line Model

The circuit transmission line model we want to determine describes the field problem in terms of voltages, currents, the complex capacitance matrix $\tilde{\mathsf{C}} = \mathsf{C} + \mathsf{G}/j\omega$, and the complex inductance matrix $\tilde{\mathsf{L}} = \mathsf{L} + \mathsf{R}/j\omega$ as

$$\frac{\partial \mathbf{i}}{\partial z} = -j\omega\tilde{\mathsf{C}}\mathbf{v} \tag{8}$$

$$\frac{\partial \mathbf{v}}{\partial z} = -j\omega\tilde{\mathsf{L}}\mathbf{i} \tag{9}$$

with $\mathbf{v}(z)$ and $\mathbf{i}(z)$ being the $N \times 1$ voltage and current vectors associated with the N signal conductors. In the absence of

Authorized licensed use limited to: AT & T. Downloaded on May 13, 2009 at 10:24 from IEEE Xplore. Restrictions apply.

a PEC reference conductor, only $N-1$ currents and voltages are needed. A large body of literature (see [12]) has been dedicated to investigate the mapping of the field problem onto a circuit description. One possible approach is to invoke power conservation together with a precise definition for either the current (PI model) or the voltage (PV model). The latter approach was also adopted in [1] for the single line case. The PI and PV model will only yield (almost) identical results in the (quasi-)TEM case. For the multiconductor case discussed here, a different approach based on reciprocity and mode orthogonality will be adopted, as explained and motivated in the sequel. For a general discussion on the differences between power- and reciprocity-based models, we refer the reader to [12]. It has to be remarked that for lossless structures, both types of models are identical as the modal fields can be chosen to be real.

Just as for the fields in (6) and (7), the voltages and currents in (8) and (9) can be expressed in terms of eigenmodes as

$$\mathbf{v}(z) = \sum_{m=1}^{N} \mathbf{v}_m \left(K_m^+ e^{-j\beta_m z} + K_m^- e^{j\beta_m z}\right) \tag{10}$$

$$\mathbf{i}(z) = \sum_{m=1}^{N} \mathbf{i}_m \left(K_m^+ e^{-j\beta_m z} - K_m^- e^{j\beta_m z}\right). \tag{11}$$

The voltage and current eigenmodes $\mathbf{v}_m$ and $\mathbf{i}_m$ are solutions to the following equations:

$$j\beta_m \mathbf{i}_m = j\omega \tilde{\mathsf{C}}\, \mathbf{v}_m \tag{12}$$

$$j\beta_m \mathbf{v}_m = j\omega \tilde{\mathsf{L}}\, \mathbf{i}_m. \tag{13}$$

The reader will remark that the eigenvalues β_m are identical in all field and circuit equations. This property of the model is quite obvious, as we require the modal signal speeds to be identical for the actual fields and for their circuit representation. Furthermore, the modal excitation coefficients K_m^+ and K_m^- are also *identical* in the modal field and modal circuit description. In general, this is only possible in reciprocity-based models by requiring that the following equality holds:

$$\iint_S (\mathbf{e}_t \times \mathbf{h}_t)\cdot \mathbf{u}_z dS = \mathbf{v}^T \cdot \mathbf{i} \tag{14}$$

with S being the total cross section and with the superindex T indicating the transpose of the vector. Expression (14) differs from the one used in power-based models in which the complex conjugate of $\mathbf{h}_t$ and $\mathbf{i}$ are used. As a consequence of the fundamental modal field orthogonality property [12] stating that

$$\iint_S (\mathbf{E}_{ti} \times \mathbf{H}_{tj})\cdot \mathbf{u}_z \, dS = 0, \qquad i \neq j \tag{15}$$

for any modal fields $\mathbf{E}_{ti}$ and $\mathbf{H}_{tj}$, (14) also remains valid on a mode per mode basis, i.e.,

$$\iint_S (\mathbf{E}_{\rm tm} \times \mathbf{H}_{\rm tm})\cdot \mathbf{u}_z dS = \mathbf{v}_m^T \cdot \mathbf{i}_m \tag{16}$$

and this property will be needed in the sequel. In the lossy case, using a power-based model, this property is lost because the modes are no longer power orthogonal, as in the lossless case.

In the following sections, starting from the above general description of the field problem and its circuit equivalent, we turn to the solution of the quasi-TM problem and to the determination of the complex capacitance and inductance matrix.

IV. Capacitance Problem and the Meaning of Voltages and Currents in the Transmission Line Equivalent

A. Theoretical Analysis

Due to the fact that $\sigma \gg \omega\epsilon$ for signal conductors, the *cross-sectional* tangential electric field $\mathbf{e}_{\rm tan}$ at the conductor's surface must be zero. If this would not be the case, the presence of such a field would very quickly (i.e., within a few times the relaxation time ϵ/σ), lead to a redistribution of the surface charges such that $\mathbf{e}_{\rm tan}$ becomes zero. $\mathbf{e}_{\rm tan}$ can be expressed in terms of the vector potential $\mathbf{a}$ and the scalar potential ϕ as $\mathbf{e}_{\rm tan} = -(\partial\phi/\partial_{\rm tan})\mathbf{u}_{\rm tan} - j\omega \mathbf{a}_{\rm tan}$. Outside the good conductors, $\mathbf{a}_t$ is of order ω, and hence, in the quasi-TM approximation, $\omega \mathbf{a}_t$ is neglected with respect to $\nabla_t \phi$ (which corresponds to neglecting h_z with respect to $\mathbf{h}_t$). The continuity of $\mathbf{a}_{\rm tan}$ at the conductor's boundary implies, therefore, that $\mathbf{e}_{\rm tan} \approx -(\partial\phi/\partial_{\rm tan})\mathbf{u}_{\rm tan}$. This, in turn, shows that, for a fixed value of z, ϕ takes a constant value on all signal conductors' boundaries, allowing to *define* the circuit voltages $\mathbf{v}$ in (9) as these constant potential values.

We will now derive a general expression for the capacitance matrix and from this infer a meaning for the circuit currents $\mathbf{i}$. Cross multiplying (3) with $\mathbf{e}_t$ and taking advantage of (2) shows that

$$\mathbf{e}_t \times \frac{\partial \mathbf{h}_t}{\partial z} = -(\sigma + j\omega\epsilon)(\mathbf{e}_t \cdot \mathbf{e}_t)\mathbf{u}_z - j\omega\mu_0 h_z^2 \mathbf{u}_z - \nabla_t \times (h_z \mathbf{e}_t). \tag{17}$$

Integrating this over the cross section S leads to the approximate result

$$\iint_S \left(\mathbf{e}_t \times \frac{\partial \mathbf{h}_t}{\partial z}\right)\cdot \mathbf{u}_z \, dS = -\iint_S (\sigma + j\omega\epsilon)\mathbf{e}_t \cdot \mathbf{e}_t \, dS. \tag{18}$$

To obtain (18), the contribution of the higher order term in h_z^2 was neglected. The $\nabla_t \times ()$ term reduces to a vanishing boundary integral at infinity or to a zero contribution on the surface of a PEC conductor when present. We now insert expansions (6) and (7) into the left-hand side of (18), invoke the mode orthogonality (15), and use (8), (10), and (11) to show that

$$-\mathbf{v}^T \cdot \frac{\partial \mathbf{i}}{\partial z} = \mathbf{v}^T \cdot (j\omega \tilde{\mathsf{C}}) \cdot \mathbf{v} = \iint_S (\sigma + j\omega\epsilon)\mathbf{e}_t \cdot \mathbf{e}_t \, dS. \tag{19}$$

Note that using the power conservation and reciprocity approach of [14]–[16] does not allow to obtain (19). It would be interesting to investigate how to modify the present theory to accommodate this alternative approach, but this falls outside the scope of this paper. The total cross section S consists of three parts, i.e.: 1) signal conductors; 2) semiconductors; and 3) dielectrics (including the background medium). For the dielectrics, the approximation $\mathbf{e}_t = -\nabla_t \phi$ holds as the contribution from the vector potential $-j\omega \mathbf{a}_t$ is of higher order in ω. For the semiconductors, the following reasoning can be adopted. For the

Authorized licensed use limited to: AT & T. Downloaded on May 13, 2009 at 10:24 from IEEE Xplore. Restrictions apply.

frequency range in which σ remains much larger than $\omega\epsilon$, the potential ϕ on the boundary of the semiconductor will remain constant, just as for a signal conductor. For these frequencies for which this no longer holds, the semiconductor will behave as a complex dielectric. The potential will not be constant on its boundary, but now (just as for the lossy dielectrics) it is allowed to state that the approximation $\mathbf{e}_t = -\nabla_t \phi$ holds. The neglected term $-j\omega \mathbf{a}_t$ is very small in the quasi-TM range and is, therefore, negligible with respect to the term $-\nabla_t \phi$. In the case of a constant boundary potential, this approximation is no longer valid, but then the *total* transverse electric field itself becomes very small. The numerical results in Section VI will confirm that the semiconductor behavior can be captured as described above.

To further transform the right-hand side (RHS) of (19), following the above reasoning, the cross section S is subdivided in two parts S_1 and S_2. S_1 encompasses the signal conductors and those semiconductors for which, at the considered frequency, the potential is constant on their boundary. S_2 is the remaining part of S and here $\mathbf{e}_t = -\nabla_t \phi$ holds. Taking into account the divergence law (5), the contribution from S_2 to the RHS of (19) becomes

$$\begin{aligned}\int\!\!\int_{S_2} &(\sigma + j\omega\epsilon)\, \mathbf{e}_t \cdot \mathbf{e}_t \, dS \\ &= -\int\!\!\int_{S_2} (\sigma + j\omega\epsilon) \left(\nabla_t \cdot (\phi\, \mathbf{e}_t) + \phi \frac{\partial e_z}{\partial z} \right) dS \qquad (20)\\ &= \int_{c_2} (\sigma + j\omega\epsilon) \phi\, \mathbf{u}_n \cdot \mathbf{e}_t \, dc - \int\!\!\int_{S_2} (\sigma + j\omega\epsilon) \phi \frac{\partial e_z}{\partial z} \, dS. \qquad (21)\end{aligned}$$

The boundary c_2 of S_2 consists of: 1) a contribution at infinity, which drops out; 2) possible contributions of dielectrics and/or semiconductors touching each other, but due to the continuity of $(\sigma + j\omega\epsilon)\, \mathbf{u}_n \cdot \mathbf{e}_t$ these contributions also drop out; and 3) contributions at the boundaries between these materials and the signal conductors and semiconductors with a constant surface potential. In the sequel, the term "relevant" is used to indicate these semiconductors. In (21), the normal $\mathbf{u}_n$ is directed outwards with respect to the good conductors, explaining the change in sign in going from (20) to (21). In these remaining contributions, i.e., 3), the constant potential can be put in front of the integration, the continuity of $(\sigma + j\omega\epsilon)\, \mathbf{u}_n \cdot \mathbf{e}_t$ can again be invoked and the divergence theorem combined with (5), but now for the cross sections of the signal conductors and the relevant semiconductors, lead to the following expression for the first term in (21):

$$\begin{aligned}\int_{c_2} (\sigma + j\omega\epsilon) \phi\, \mathbf{u}_n \cdot \mathbf{e}_t \, dc &= -\sum_j \phi_j \frac{\partial}{\partial z} \int\!\!\int_{S_j} \sigma e_z \, dS \qquad (22)\\ &= -\sum_j \phi_j \frac{\partial I_j}{\partial z} \qquad (23)\\ &= j\omega \sum_j \phi_j q_j. \qquad (24)\end{aligned}$$

The summation in (24) now runs over all signal conductor cross sections *and* relevant semiconductor cross sections, ϕ_j is the constant potential, I_j is the total longitudinal current, and q_j is the total surface charge associated with cross section j. To avoid confusion with the circuit currents $\mathbf{i}$ introduced in (8) and (9), we use capital I's here. To obtain (24) and in line with previous approximations, displacement currents in good conducting materials were neglected with respect to conduction currents. We now turn back to (19) and write it with (21) and (24) as

$$\mathbf{v}^T \cdot (j\omega \tilde{\mathsf{C}}) \cdot \mathbf{v} = j\omega \sum_j \phi_j q_j - \int\!\!\int_{S_2} (\sigma + j\omega\epsilon) \phi \frac{\partial e_z}{\partial z} \, dS + \int\!\!\int_{S_1} \sigma \mathbf{e}_t \cdot \mathbf{e}_t \, dS. \qquad (25)$$

To keep our approximations consistent, comparing (22) and the remaining integral over S_2 in (25), we see that we have to drop this term because the longitudinal conduction and displacement currents in S_2 are much smaller than the currents in the signal conductors. Moreover, the last term of (25) stands for the contribution from transversal currents in the good conducting materials, and these remain negligible as compared to the contribution of the longitudinal currents represented by the second term. Hence, from (25), we finally arrive at

$$\mathbf{v}^T \cdot \tilde{\mathsf{C}} \cdot \mathbf{v} = \begin{bmatrix} \mathbf{v}^T & \mathbf{v}_{\mathrm{sc}}^T \end{bmatrix} \cdot \begin{bmatrix} \mathbf{q} \\ \mathbf{q}_{\mathrm{sc}} \end{bmatrix} \qquad (26)$$

with $\mathbf{q}$ and $\mathbf{q}_{\mathrm{sc}}$ column vectors containing the charges, respectively, on each signal conductor and on each relevant semiconductor and with $\mathbf{v}$ and $\mathbf{v}_{\mathrm{sc}}$ containing the corresponding voltages. The voltages $\mathbf{v}_{\mathrm{sc}}$ depend linearly on $\mathbf{v}$.

According to (26), the capacitance matrix can be obtained solving an almost classical capacitance problem. We will come back to that problem in Section IV-B. Suffices to say here that two distinct situations can occur. Either one of the relevant semiconductors touches a signal conductor such that its potential becomes equal to that of the signal conductor, or the semiconductor stands free, but in that case, its total charge must remain zero. Together with Laplace's equation for the potential, this will suffice to determine $\tilde{\mathsf{C}}$. Using (8), (26) can also be rewritten as

$$\mathbf{v}^T \cdot \frac{\partial \mathbf{i}}{\partial z} = \begin{bmatrix} \mathbf{v}^T & \mathbf{v}_{\mathrm{sc}}^T \end{bmatrix} \cdot \begin{bmatrix} \dfrac{\partial \mathbf{I}}{\partial z} \\ \dfrac{\partial \mathbf{I}_{\mathrm{sc}}}{\partial z} \end{bmatrix}. \qquad (27)$$

From the above equation, we can now derive the following interpretation for the circuit currents $\mathbf{i}$ in our reciprocity-based quasi-TM model. Suppose that signal conductor n is put at the nonzero potential v_n while all other signal conductor potentials remain zero. From (27), we see that

$$i_n = I_n + \sum_p \frac{v_{\mathrm{sc,p}}}{v_n} I_{\mathrm{sc},p}. \qquad (28)$$

This shows that the circuit current i_n associated with signal conductor n must be interpreted as the actual current running through that conductor increased by suitably weighted currents running through some of the relevant semiconductors. From the semiconductors taken into account as good conductors, only

Authorized licensed use limited to: AT & T. Downloaded on May 13, 2009 at 10:24 from IEEE Xplore. Restrictions apply.

those remain present in the summation over p provided they touch the considered signal conductor such that $v_{\text{sc},p} = v_n$. In all other cases, their contribution remains zero either because they touch a signal conductor at zero potential $v_{\text{sc},p} = 0$ or are standing free, in which case $I_{\text{sc},p} = 0$. Above, a lot of, but consistent, approximations have been introduced. Such approximations are inevitable when trying to come up with a quasi-TM analysis.

In [1], for the single signal conductor case $N = 1$, power conservation was invoked to derive an expression for the circuit current i associated with a voltage excitation v, leading to a current expression [1, eq. (27)] differing from the traditional conduction current found in the following quasi-TEM approximation:

$$i = i_c + \iint_{S_{\text{semiconductor}}} J_z \frac{\phi^*}{v^*} \, dS. \tag{29}$$

The current i is the sum of the total longitudinal current i_c flowing in the signal conductor and a, by the normalized complex conjugate potential ϕ^*/v^* of the semiconductors, weighted contribution of the longitudinal currents flowing in the semiconducting layers. If we keep the potential under the integral sign in the contribution of the semiconductors in (25), a similar result is obtained. For the examples considered in [1], our numerical results (see Section VI) are identical. This is a consequence of: 1) the fact that the semiconductor contributions to (29) are indeed negligible when their potential is not constant and 2) the fact that their contribution is identically zero when the potential is constant because, in the numerical examples in [1], all semiconductors touch the ground conductor and/or the surrounding metallic box, which are kept at zero potential.

B. Numerical Solution

The capacitance problem formulated above can numerically be solved by various techniques. Here we opt for a surface integral-equation solution combined with the Dirichlet to Neumann operator presented in [17], but specifically tailored to the capacitance problem. To this end, all materials are replaced by their equivalent unknown contrast current source $\mathbf{j}_c = (\sigma + j\omega(\epsilon - \epsilon_0))\,\mathbf{e}$. These sources reside in the homogeneous background medium and generate the original fields. The z-component of this contrast current will serve as the starting point for solving the inductance problem in Section V, and the transverse component is essential for the capacitance problem.

As all media are piecewise homogeneous, the divergence of $\mathbf{j}_c$ is zero and no volume contrast charges are present. However, at each interface between a material and the background medium, a contrast surface charge density ρ_{sc}, given by

$$\rho_{\text{eq}} = -\frac{j_{\text{cn}}}{j\omega} = -\left(\epsilon - \epsilon_0 + \frac{\sigma}{j\omega}\right) e_n \tag{30}$$

must be taken into account, with j_{cn} and e_n representing the normal components with regard to the outward pointing unit normal $\mathbf{u}_n$. The equivalent surface charge ρ_{eq} in (30) consists of the actual surface charge and of the so-called polarization surface charge with respect to the homogeneous background medium. In reality, more complex situations such as the interface between a dielectric and a signal conductor or semiconductor will occur. In these cases, two contrast surface densities ρ_{sc}^+ and ρ_{sc}^- are introduced, each defined as in (30) with respect to the outward pointing normal. The sum of ρ_{sc}^+ and ρ_{sc}^- yields the correct total contrast surface charge. Neglecting $\epsilon - \epsilon_0$ with respect to $(\sigma/j\omega)$ in (30) at good conductors and relevant semiconductors (completely in line with the reasoning in Section IV-A), we immediately see that the total contrast surface charges on these constant potential surfaces are those needed in (26).

Now consider the potential ϕ_{eq} due to all introduced contrast surface charge densities. This potential differs from the potential ϕ introduced in Section IV-A, but throughout the cross section of each good conductor or relevant semiconductor, ϕ_{eq} assumes the same constant value as ϕ on its boundary. As the contrast charges reside in a homogeneous background medium, ϕ_{eq} satisfies Laplace's equation everywhere and can, hence, be expressed as

$$\phi_{\text{eq}}(\boldsymbol{r}) = -\frac{1}{\epsilon_0} \int_{\Sigma c} \rho_{\text{eq}}(\boldsymbol{r}') G_0(\boldsymbol{r}|\boldsymbol{r}') \, dc(\boldsymbol{r}'). \tag{31}$$

The integration runs over all the boundaries c on which contrast charges were introduced. The Green's function G_0 satisfies

$$\nabla_t^2 G_0(\boldsymbol{r}|\boldsymbol{r}') + (k_0^2 - \beta^2) G_0(\boldsymbol{r}|\boldsymbol{r}') = \delta(\boldsymbol{r} - \boldsymbol{r}') \tag{32}$$

with k_0 being the wavenumber of the background medium. The term $-\beta^2 G_0(\boldsymbol{r}|\boldsymbol{r}')$ stands for the second-order derivative with respect to z, and as long as the quasi-TM assumption holds, it is negligible with respect to each of the transverse second-order derivatives in $\nabla_t^2 G_0(\boldsymbol{r}|\boldsymbol{r}')$. As k_0^2 has the same order of magnitude as β^2, it is neglected as well and (32) reduces to

$$\nabla_t^2 G_0(\boldsymbol{r}|\boldsymbol{r}') = \delta(\boldsymbol{r} - \boldsymbol{r}'). \tag{33}$$

The quasi-static Green's function G_0 is equal to $(1/2\pi)\ln|\boldsymbol{r} - \boldsymbol{r}'|$ for free space. If we consider a half-plane on top of a PEC ground, an image source term $-\delta(\boldsymbol{r} - \boldsymbol{r}'')$ (with $\boldsymbol{r}''$ being the mirror image of $\boldsymbol{r}'$ with respect to the PEC ground) is added to the RHS of (32) and (33), and G_0 becomes $(1/2\pi)\ln(|\boldsymbol{r} - \boldsymbol{r}'|/|\boldsymbol{r} - \boldsymbol{r}''|)$. For $\boldsymbol{r}$ on c in (31), a surface integral equation for ρ_{eq} is obtained.

The relevant semiconductors can be subdivided into two groups regardless of whether or not they are attached to a signal conductor. The potential of those that touch a signal conductor is equal to that of the signal conductor (i.e., zero for a semiconductor touching a PEC reference conductor). The total charge on each of the signal conductors and the total charge of the attached relevant semiconductors is denoted as $(\mathbf{q} + \mathbf{q}_{\text{sc},A})$. The charge and potential of the relevant semiconductors that stand free are written as $\mathbf{q}_{\text{sc},F}$, respectively, $\mathbf{v}_{\text{sc},F}$. With this notation, (26) can be transformed into

$$\mathbf{v}^T \cdot \tilde{\mathsf{C}} \cdot \mathbf{v} = \begin{bmatrix} \mathbf{v}^T & \mathbf{v}_{\text{sc},F}^T \end{bmatrix} \cdot \begin{bmatrix} \mathbf{q} + \mathbf{q}_{\text{sc},A} \\ \mathbf{q}_{\text{sc},F} \end{bmatrix}. \tag{34}$$

To obtain all the elements of the capacitance matrix, one by one we put $\phi_{\text{eq}} = 1$ on the boundary of a signal conductor and its touching constant surface potential semiconductors, as well

Authorized licensed use limited to: AT & T. Downloaded on May 13, 2009 at 10:24 from IEEE Xplore. Restrictions apply.

as on the relevant semiconductors that are standing free, while keeping $\phi_{\rm eq} = 0$ on all the other ones, each time solving (31). In this way, the extended capacitance matrix defined as

$$\begin{bmatrix} \mathbf{q} + \mathbf{q}_{{\rm sc},A} \\ \mathbf{q}_{{\rm sc},F} \end{bmatrix} = \tilde{\mathsf{C}}_{\rm ext} \cdot \begin{bmatrix} \mathbf{v} \\ \mathbf{v}_{{\rm sc},F} \end{bmatrix} \tag{35}$$

is obtained. Once $\tilde{\mathsf{C}}_{\rm ext}$ is determined, the actual capacitance matrix $\tilde{\mathsf{C}}$ can be retrieved after some straightforward matrix manipulations by eliminating $\mathbf{v}_{{\rm sc},F}$ and $\mathbf{q}_{{\rm sc},F}$ from (35) based on the requirement that when a semiconductor stands free, its total charge remains zero, and thus, $\mathbf{q}_{{\rm sc},F} = 0$. However, fixing the boundary potentials as explained above does not suffice to solve (31). For this, additional relationships between the potentials and the charges on the remaining boundaries are needed, more specifically on the boundaries of the dielectrics and the semiconductors, which behave as lossy dielectrics. We focus our attention to such a single homogeneous semiconductor with cross section S_i and boundary c_i. In this case, the original potential ϕ in S_i approximately satisfies $\nabla_t^2 \phi = j\omega\mu_0\sigma\phi$. The diffusion term is present if σ becomes significantly larger than $\omega\epsilon$, even when not yet high enough for ϕ to become constant on the boundary. In this case, as explained in Section IV-A, the approximation $\mathbf{e}_t = -\nabla_t \phi$ (i.e., dropping the higher order contribution $-j\omega\mathbf{a}_t$ of the vector potential) is still valid, as is the case for dielectrics. Let us now expand ϕ in terms of the normalized Dirichlet eigenfunctions ξ_m of S_i, which themselves satisfy

$$\nabla_t^2 \xi_m(\boldsymbol{r}) + k_m^2 \xi_m(\boldsymbol{r}) = 0, \qquad \boldsymbol{r} \in S_i \tag{36}$$

with $\xi_m = 0$ on the boundary c_i of S_i and with k_m^2 on the corresponding Dirichlet eigenvalues. It is easily derived that the normal derivative $(\partial\phi/\partial n)$ can be expressed as

$$\frac{\partial \phi(\boldsymbol{r})}{\partial n} = -\frac{\partial}{\partial n} \sum_{\forall m} \frac{\xi_m(\boldsymbol{r})}{k_m^2 + j\omega\mu_0\sigma} \oint_{c_i} \phi(\boldsymbol{r}') \frac{\partial \xi_m(\boldsymbol{r}')}{\partial n}\, dc(\boldsymbol{r}') \tag{37}$$

with $\boldsymbol{r} \in c_i$. For lossless dielectrics, the term $j\omega\mu_0\sigma$ is not present. Relationship (37) between $(\partial\phi/\partial n)$ and ϕ is a Dirichlet to Neumann boundary operator. Going back to (30) and approximating e_n by $-(\partial\phi/\partial n)$, (30) and (37) yield a relationship between the contrast charge density and the potential on c_i. Discretization of this relationship and of (31) with the MoM yields the wanted charge distributions and the elements of $\tilde{\mathsf{C}}_{\rm ext}$.

Note that the integral (31) combines the *equivalent* potential $\phi_{\rm eq}$ with the contrast charge density. On the RHS of (37), ϕ is, therefore, replaced by $\phi_{\rm eq}$. This is allowed on all boundaries with good conductors (with constant potential $\phi = \phi_{\rm eq}$ on the outer boundary), and on all boundaries with dielectrics (where $\phi = \phi_{\rm eq}$ as well). On internal boundaries between two touching semiconductors that both exhibit an important conductivity, ϕ is subject to diffusion, whereas $\phi_{\rm eq}$ is not, and hence, $\phi_{\rm eq} \neq \phi$. However, if the potential is not yet constant on the outer boundary, the diffusion is still limited and the small difference between ϕ and $\phi_{\rm eq}$ has very little influence on the solution to the integral equation.

At this point, we will not discuss the numerical method in further detail. It suffices to mention that the relation between $\rho_{\rm eq}$ and $\phi_{\rm eq}$ on the boundaries is discretized in an analogous way as the differential surface admittance operator $\mathcal{Y}$ in [17], although here, piecewise linear basis functions were used to discretize both quantities, whereas [17] uses pulse functions.

V. Inductance Problem

To solve the inductance problem, we will only need the longitudinal part of the contrast current, i.e., $j_{c,z} = (\sigma + j\omega(\epsilon - \epsilon_0))\, e_z = (k_0^2 - k^2)\, e_z / j\omega\mu_0$ with e_z the as yet unknown longitudinal electric field and k the wavenumber of the considered material. First, we will restrict the reasoning to a particular mode m and afterwards extend the result to an arbitrary superposition of modes. To distinguish between the single mode problem and the general one, capital letters will be used for the modal problem. The scalar vector potential A_{zm} for the equivalent contrast current problem is

$$-j\omega A_{zm}(\boldsymbol{r}) = \int\!\!\int_{\Sigma S_i} \left((k_0^2 - \beta_m^2) - (k^2 - \beta_m^2) \right) \cdot E_{zm}(\boldsymbol{r}') G_0(\boldsymbol{r}|\boldsymbol{r}')\, dS(\boldsymbol{r}'). \tag{38}$$

The integration runs over all the cross sections S_i of the different materials. The longitudinal electric field E_{zm} satisfies the wave equation

$$\nabla_t^2 E_{zm} + (k^2 - \beta_m^2) E_{zm} = 0 \tag{39}$$

and can be written in terms of the potentials as

$$E_{zm}(\boldsymbol{r}) = j\beta_m \phi_{{\rm eq},m}(\boldsymbol{r}) - j\omega A_{zm}(\boldsymbol{r}) \tag{40}$$

where $\phi_{{\rm eq},m}$ is the equivalent scalar potential for mode m and with $\phi_{\rm eq}$ the same equivalent potential as already introduced in Section IV-B. Judicious manipulations of (38) and (40), invoking (32) and (39) in conjunction with Green's theorem, lead to

$$j\beta_m \phi_{{\rm eq},m}(\boldsymbol{r}) = -\int_{\Sigma c_j} \left(\frac{\partial E_{zm}(\boldsymbol{r}')}{\partial n} G_0(\boldsymbol{r}|\boldsymbol{r}') - E_{zm}(\boldsymbol{r}') \frac{\partial G_0(\boldsymbol{r}|\boldsymbol{r}')}{\partial n} \right) dc(\boldsymbol{r}'). \tag{41}$$

Next we introduce the fictitious field E_{z0m} within each subregion S_i, defined as a solution to the homogeneous wave equation (i.e., without the contrast current source term) in the background medium, i.e.,

$$\nabla_t^2 E_{z0m} + (k_0^2 - \beta_m^2) E_{z0m} = 0 \tag{42}$$

and which takes the same value $E_{z0m} = E_{zm}$ on the boundary and only on the boundary c_i of S_i as the E_{zm} field we want to determine. This allows to write (41) for any observation point $\boldsymbol{r}$, again using (32), as

$$E_{z0m}(\boldsymbol{r}) = j\beta_m \phi_{{\rm eq},m}(\boldsymbol{r}) + \int_{\Sigma c_j} \left(\frac{\partial E_{zm}(\boldsymbol{r}')}{\partial n} - \frac{\partial E_{z0m}(\boldsymbol{r}')}{\partial n} \right) \cdot G_0(\boldsymbol{r}|\boldsymbol{r}')\, dc(\boldsymbol{r}'). \tag{43}$$

In the quasi-TM limit, the integration runs over all boundaries c_j of conductors and semiconductors. The dielectrics yield no contribution because E_{zm} and E_{z0m} have the same boundary value and satisfy Laplace's equation, which amounts to neglecting the

Authorized licensed use limited to: AT & T. Downloaded on May 13, 2009 at 10:24 from IEEE Xplore. Restrictions apply.

dielectric displacement currents in (38), as compared to the conductors' currents. Physically, as introduced in [17], (43) means that the inductance problem can be described in terms of equivalent so-called differential surface currents on each boundary c_j given by

$$J_{sm,j}(\boldsymbol{r}') = \frac{1}{j\omega\mu_0}\left(\frac{\partial E_{zm}(\boldsymbol{r}')}{\partial n'} - \frac{\partial E_{z0m}(\boldsymbol{r}')}{\partial n'}\right) \tag{44}$$

with $\boldsymbol{r}' \in c_j$. It has also been shown in [17] that the following differential surface admittance operator $\mathcal{Y}(\boldsymbol{r}', \boldsymbol{r}'')$ can be introduced:

$$J_{sm,j}(\boldsymbol{r}') = \oint_{c_j} \mathcal{Y}_j(\boldsymbol{r}', \boldsymbol{r}'') E_{zm,j}(\boldsymbol{r}'')\, dc(\boldsymbol{r}''), \qquad \boldsymbol{r}' \in c_j \tag{45}$$

expressing a relationship between the differential surface current on boundary c_j and the longitudinal electric field on that same boundary. Note that in the quasi-TM limit, the operator $\mathcal{Y}$ does *not* depend on β_m, as in this limit we approximate $(k^2 - \beta_m^2)$ in (39) by $-j\omega\mu_0\sigma$ and neglect the term $(k_0^2 - \beta_m^2)E_{z0m}$ in (42) with respect to both terms in $\nabla_t^2 E_{z0m}$. Integrating $J_{sm,j}$ over c_j leads to an expression for the longitudinal current I_j through the cross section S_j

$$I_{jm} = \oint_{c_j} J_{sm,j}(\boldsymbol{r}')\, dc(\boldsymbol{r}'). \tag{46}$$

Until now, the reasoning was restricted to a particular mode, meaning that the signal conductor potentials ϕ_{eq} take their respective modal values on each of the signal conductors. To extend (43) to a general superposition of modes, we start from (13) and consider an arbitrary superposition of modes corresponding to a set of voltages $\mathbf{v}$ used to excite the signal conductors to arrive at

$$\tilde{\mathsf{L}}^{-1} \sum_m \alpha_m \mathbf{v}_m = \tilde{\mathsf{L}}^{-1}\, \mathbf{v} = j\omega \sum_m \alpha_m \frac{\mathbf{i}_m}{j\beta_m}. \tag{47}$$

The α_m's are modal amplitudes. If we now define the following quantities:

$$\hat{e}_{z0} = \sum_m \alpha_m \frac{E_{z0m}}{j\beta_m} \tag{48}$$

$$\phi_{\text{eq}} = \sum_m \alpha_m \phi_{eq,m} \tag{49}$$

$$\hat{i}_p = \sum_m \alpha_m \frac{i_{m,p}}{j\beta_m}. \tag{50}$$

Equations (45), (43), and (46) can be rewritten as

$$\hat{j}_{s,j}(\boldsymbol{r}') = \oint_{c_j} \mathcal{Y}_j(\boldsymbol{r}', \boldsymbol{r}'') \hat{e}_{z0}(\boldsymbol{r}'')\, dc(\boldsymbol{r}'') \tag{51}$$

$$\hat{e}_{z0}(\boldsymbol{r}) = \phi_{\text{eq}}(\boldsymbol{r}) + j\omega\mu_0 \cdot \oint_{\Sigma c_j} \hat{j}_{s,j}(\boldsymbol{r}') G_0(\boldsymbol{r}|\boldsymbol{r}')\, dc(\boldsymbol{r}') \tag{52}$$

$$\hat{I}_j = \oint_{c_j} \hat{j}_{s,j}\, dc. \tag{53}$$

We now turn back to (47) and put signal conductor n on potential v_n with all other signal conductors on zero potential, leading to

$$\left[\tilde{\mathsf{L}}^{-1}\right]_{pn} = \frac{j\omega}{v_n}\, \hat{i}_p. \tag{54}$$

To obtain the wanted elements of the inverse of the inductance matrix, the knowledge of the weighted circuit currents $\hat{i}_p$ suffices. In Section IV, these circuit currents (28) were found as a suitable combination of the currents I_n running through the signal conductors and those $I_{\text{sc},p}$ running through the semiconductors. From (51)–(53), the various currents can be determined by solving the integral equation, which follows directly from (52) by putting the observation point $\boldsymbol{r}$ on the boundary of one of the conductors or semiconductors (and on which $\hat{e}_{z0} = \hat{e}_z$). For a correct solution, it is important not only to take into account those semiconductors that behave as good conductors and whether or not contribute to the circuit currents, but also those for which σ is significant, even though ϕ_{eq} is not constant yet. The required value of ϕ_{eq} can be found as a side result from the solution of the capacitance problem. Integral equation (52) is of the same form as the one obtained in [17] and can be solved using the MoM, together with the MoM discretization of (51) and the explicit calculation of $\mathcal{Y}_j$ again using the Dirichlet to Neumann operator. Knowledge of β_m is not necessary. Note, however, that once the capacitance and inductance matrix have been determined, the β_m^2/ω^2 values can be obtained as the eigenvalues of $\tilde{\mathsf{L}}\tilde{\mathsf{C}}$.

VI. Numerical Results

To validate the proposed theoretical model for the semiconductors' behavior in interconnect structures, a number of single-conductor lines are investigated. A more complicated example for a multiconductor line structure is given as well, modeling four coupled differential pair transmission lines in a realistic high-frequency chip technology.

A. MIS Microstrip Line

As a first example, consider the open MIS microstrip line, shown in the inset of Fig. 2. The line consists of a $h_1 = 500\,\mu$m-thick lossy substrate with conductivity σ_1, separated from a thin signal conductor by a lossless dielectric layer with thickness $h_2 = 135\,\mu$m. All materials are nonmagnetic (as will be the case in all the examples). Simulations were performed at 1 GHz for increasing values of σ_1 such that the fundamental mode evolves from a dielectric mode, over the slow-wave range, to a skin-effect mode. In [1], an infinitely thin and PEC signal line was used. Our simulation of the PEC line (full line in Fig. 2) yields identical results for the attenuation constant α. Yet a small difference in the effective relative permittivity $\epsilon_{r,\text{eff}}$ is noticeable because the results shown here were obtained by leaving away the top side of the box surrounding the structure in [1], resulting in a small shift of the inductance, and hence, the observed difference in $\epsilon_{r,\text{eff}}$. The difference is very small though, and the large box described in [1] allows a good approximation of the open line structure. Simulating the signal line as a copper conductor ($\sigma_{\text{Cu}} = 58$ MS/m) of the same width and with finite thickness ($w = 600\,\mu$m, $t = 20\,\mu$m) only

Authorized licensed use limited to: AT & T. Downloaded on May 13, 2009 at 10:24 from IEEE Xplore. Restrictions apply.

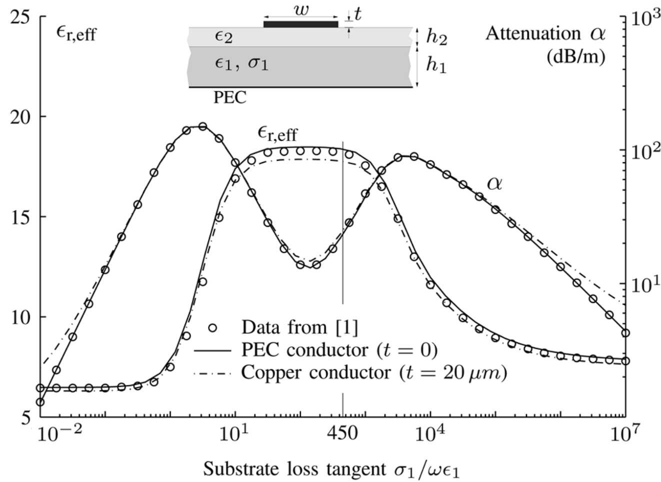

Fig. 2. Effective relative permittivity $\epsilon_{r,\mathrm{eff}}$ and attenuation coefficient (dB/m) for the fundamental mode of the shown MIS microstrip line at 1 GHz as a function of the loss tangent $\sigma_1/\omega\epsilon_1$ of the lower substrate. $w = 600\,\mu$m, $h_1 = 500\,\mu$m, $h_2 = 135\,\mu$m, and $\epsilon_1 = \epsilon_2 = 9.7\,\epsilon_0$. The vertical line indicates where $\sigma_1 = 450\,\omega\epsilon_1$.

slightly affects the results, as shown in Fig. 2 (dashed–dotted lines).

The transition between the regions in which a different semiconductor model is applied is for all examples chosen to be $\sigma_1 = 450\,\omega\epsilon_1$. For lower values of σ_1, the substrate is treated as a lossy dielectric, and for higher σ_1, as a conductor with constant surface potential. As can be seen from Fig. 2, our approach leads to correct and continuous results, as predicted by our theory.

As an illustration of the frequency dependency, the same configuration was simulated both for the PEC and the copper signal line at the frequencies of 10 MHz and 1 GHz. Fig. 3(a) shows that the resulting $\epsilon_{r,\mathrm{eff}}$ values are very similar be it that, at 10 MHz, the skin-effect mode is never reached (current crowding would only occur for a loss tangent, higher than 10^7). In both cases, there is virtually no difference in $\epsilon_{r,\mathrm{eff}}$ between the copper and the PEC conductor. However, now consider an analogous configuration, but with a smaller conductor, closer to the substrate ($h_2 = 13.5\,\mu$m, $w = 60\,\mu$m, and $t = 2\,\mu$m for the copper strip). The thickness of the lower substrate and the material parameters remain unchanged. Fig. 3(b) shows that, at 1 GHz, the finite conductivity of the line still has no influence on the propagation constant. The main difference between both configurations at 1 GHz is the different value of $\epsilon_{r,\mathrm{eff}}$ in the slow-wave range of the fundamental mode. In Fig. 3(b), $\epsilon_{r,\mathrm{eff}}$ at 1 GHz is higher than in Fig. 3(a) because the lower substrate has a higher internal inductance (as it was not scaled together with the line), whereas the capacitance remains unchanged as soon as $\sigma_1 > \omega\epsilon_1$. At 10 MHz, $\epsilon_{r,\mathrm{eff}}$ is much larger in Fig. 3(b) than in Fig. 3(a), although only for the copper conductor. By decreasing the dimensions of the line, the resistance R increases with respect to the inductance L and the point where $R \approx \omega L$ shifts towards higher frequencies. At 10 MHz, the line in Fig. 3(b) operates in the so-called *RC* range $(R > \omega L)$.

B. MIS Coplanar Waveguide (CPW)

Another single line structure, used to verify the validity of our method, is the MIS CPW presented in Fig. 4. This structure has previously been analyzed in [19] with the full-wave MoL technique, and in [1] with a quasi-TM approach (MoM/MoL). The resulting slow-wave factor (SWF) and the attenuation, obtained for a very weakly and a weakly doped substrate ($\rho = 1\,\mathrm{k}\Omega\cdot$cm, respectively, $\rho = 1\,\Omega\cdot$cm), corresponding to a dielectric and a slow-wave fundamental mode, are presented in Fig. 5 together with the results from [19] and [1]. For the heavily doped case, the characteristic impedance is shown in Fig. 6 and compared with measured values from [10] with a satisfying match.

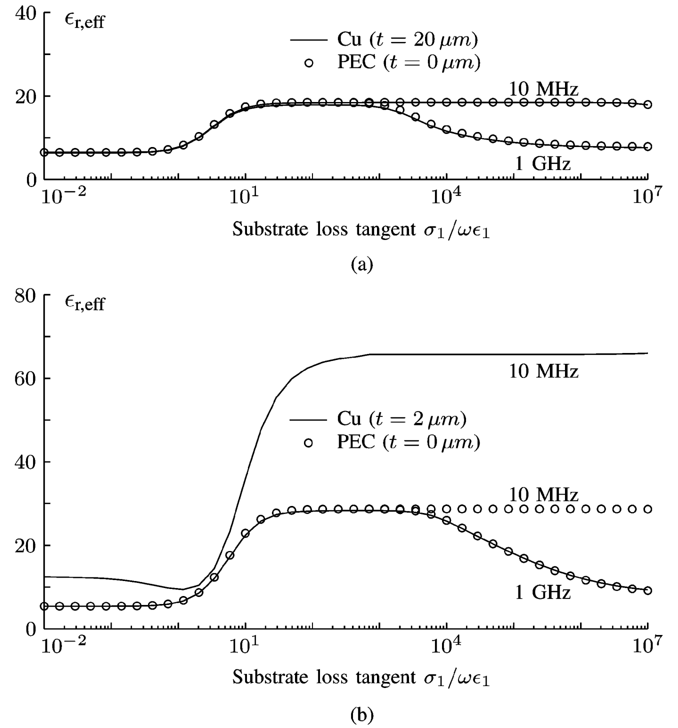

Fig. 3. $\epsilon_{r,\mathrm{eff}}$ at 10 MHz and 1 GHz for: (a) the configuration as in Fig. 2 ($h_1 = 500\,\mu$m, $h_2 = 135\,\mu$m, $w = 600\,\mu$m) and (b) a modified configuration with smaller conductor ($h_1 = 500\,\mu$m, $h_2 = 13.5\,\mu$m, $w = 60\,\mu$m).

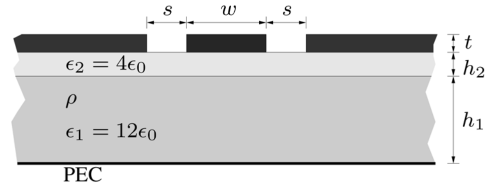

Fig. 4. MIS CPW structure (example VI-B).

C. Multiconductor Line Structure

In the final example of Fig. 7, a transmission line system of eight coupled lines is analyzed. The dimensions are based on a currently used semiconductor technology. Four identical pairs of conductors (c_1 to c_8) and a reference conductor (c_R), all with conductivity $\sigma_{\mathrm{sig}} = 40$ MS/m, are embedded in a dielectric layer above a thick semiconducting substrate on top of a PEC plane. The substrate conductivity $\sigma_{\mathrm{sub}} = 2$ S/m, unless indicated differently (as for Figs. 9 and 10). Locally (underneath c_1 and c_2), the substrate has been heavily doped ($\sigma_{\mathrm{dop}} = 0.03$ MS/m). Permittivities are $\epsilon_{\mathrm{diel}} = 4\epsilon_0$ and $\epsilon_{\mathrm{sub}} = 12\epsilon_0$. The dimensions, in micrometers, are indicated in the cross section (not shown in proportion). The structure is enclosed between

Authorized licensed use limited to: AT & T. Downloaded on May 13, 2009 at 10:24 from IEEE Xplore. Restrictions apply.

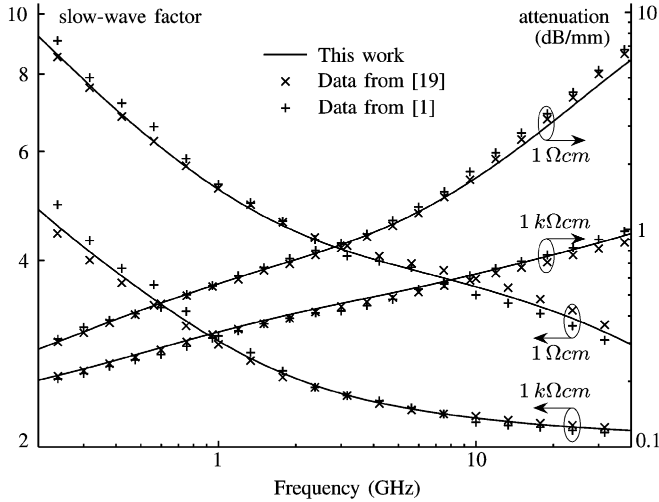

Fig. 5. SWF and attenuation for the fundamental mode in the MIS CPW of Fig. 4 with dimensions $h_1 = 480, h2 = 1, t = 0.8, s = 5, w = 10$ (all in micrometers). Top conductors: $\sigma = 27$ MS/m. Results are shown for a very weakly doped ($\rho = 1\,\mathrm{k}\Omega \cdot \mathrm{cm}$) and a weakly doped ($\rho = 1\,\Omega \cdot \mathrm{cm}$) substrate.

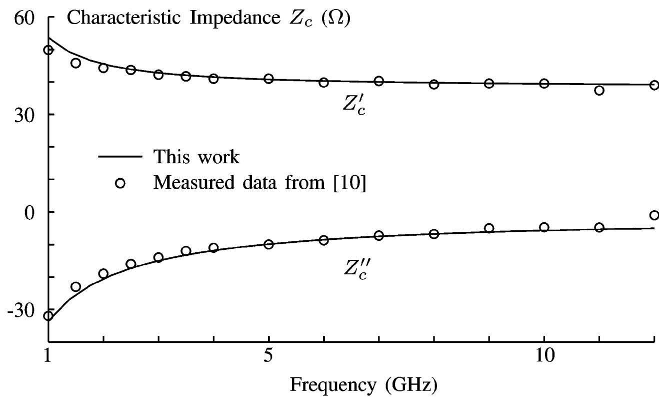

Fig. 6. Real part Z'_c and imaginary part Z''_c of the characteristic impedance for the fundamental mode in the MIS CPW from Fig. 4, with heavily doped substrate ($\rho = 0.0125\,\Omega \cdot \mathrm{cm}$). Dimensions are $h_1 = 530, h2 = 0.53, t = 1, s = 6, w = 4.2$ (all in micrometers). Top conductors: $\sigma = 33.3$ MS/m.

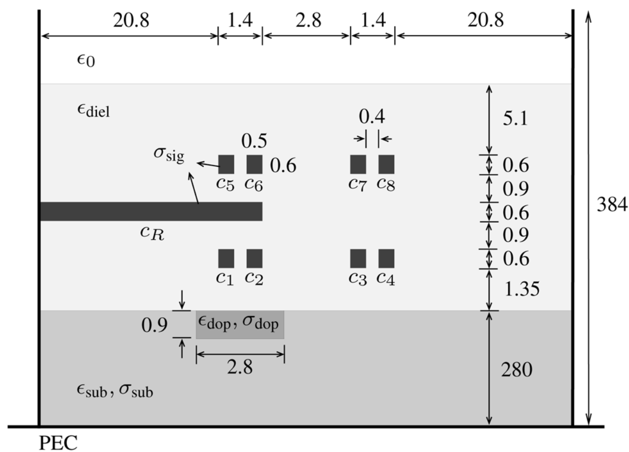

Fig. 7. Cross section of the multiconductor line structure of the example of Section VI-C. All indicated dimensions are in micrometers.

two PEC "mirror" walls at the left and right sides, in order to imitate a wide slab (as was done in [1] as well).

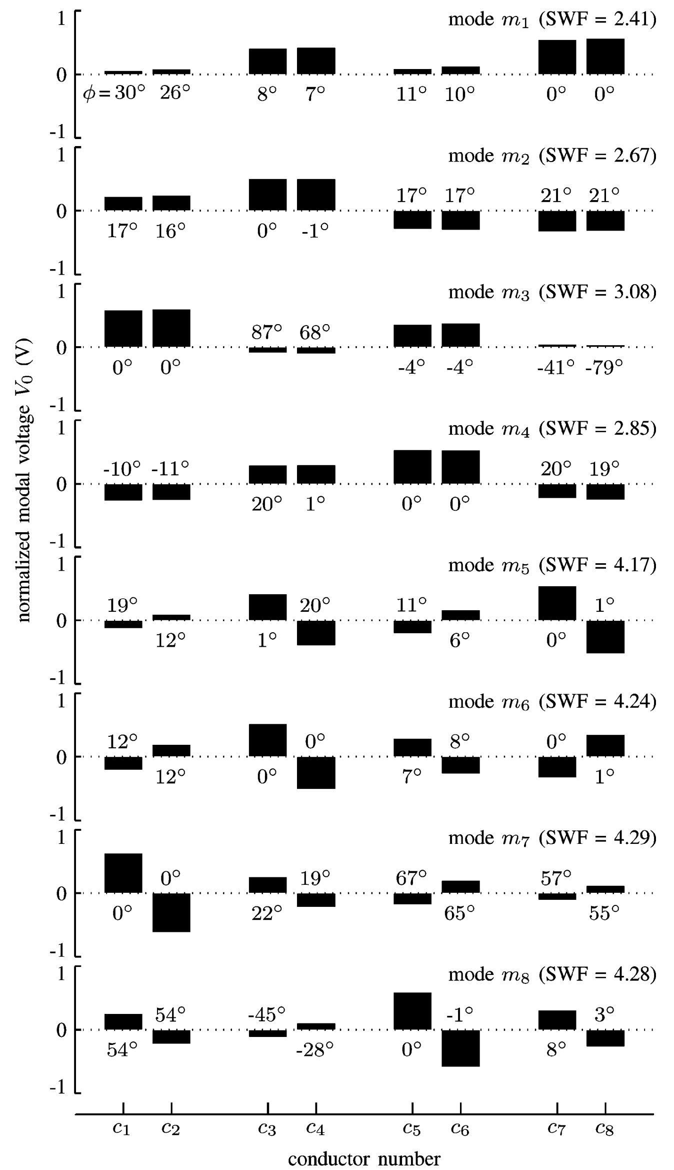

Fig. 8. Modal voltages for the configuration of Fig. 7 at 10 GHz, and with $\sigma_{\mathrm{sub}} = 2$ S/m. The complex modal voltages V are found as $V = V_0\,e^{-j\phi}$ with V_0 shown as bars and ϕ (expressed in degrees) at the corresponding bar. The modes can be split up into a quasi-"even" excitation of each of the conductor pairs (from mode m_1 to m_4), and a quasi-"odd" excitation (from mode m_5 to m_8). For each mode, the SWF is indicated as well.

In Fig. 8, the modal voltages on each signal conductor are presented for the eight fundamental modes at a frequency of 10 GHz, and for a substrate conductivity $\sigma_{\mathrm{sub}} = 2$ S/m. For a clear graphical presentation of the modes, each normalized modal voltage V is presented with a modified amplitude $V_0 = |V| \cdot \mathrm{sign}(\mathrm{Re}\,(V))$ and a phase ϕ such that $V = V_0\,e^{-j\phi}$. The modes fall apart into two groups: the modes (m_1–m_4), in which both conductors of each pair have more or less the same excitation, and those (m_5–m_8), with an opposite excitation of both conductors of each pair. In the next paragraphs, they are, respectively, called the *even* and *odd* modes.

The behavior of the SWF and attenuation as a function of the substrate loss factor $\sigma_{\mathrm{sub}}/\omega\epsilon_{\mathrm{sub}}$ is shown in Fig. 9. There is a large difference in the behavior of the even and odd modes,

Authorized licensed use limited to: AT & T. Downloaded on May 13, 2009 at 10:24 from IEEE Xplore. Restrictions apply.

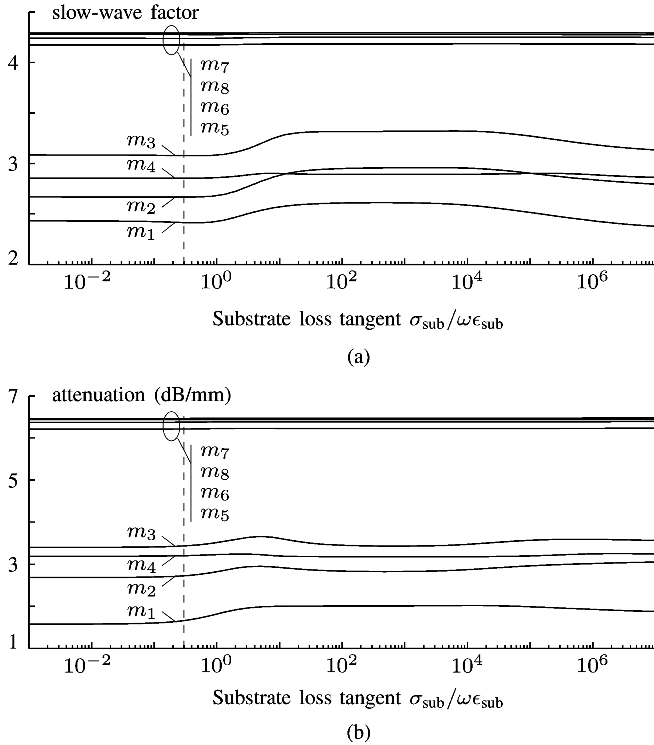

Fig. 9. (a) SWF and (b) attenuation constant for each of the fundamental modes of the multiconductor structure of Fig. 7 at 10 GHz as a function of the substrate loss tangent (ranging from 10^{-3} to 10^7). The vertical dashed lines indicate where $\sigma_{\text{sub}} = 2$ S/m, i.e., for which the modal voltages are shown in Fig. 8.

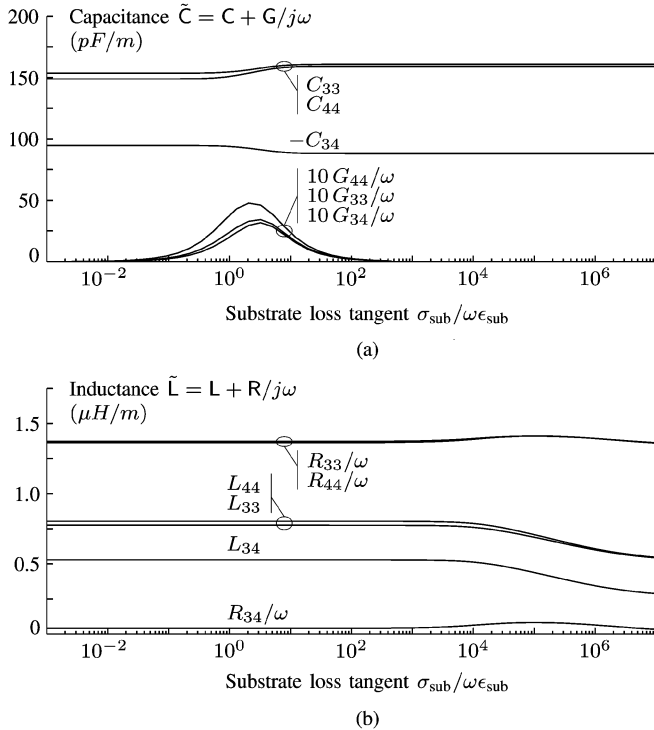

Fig. 10. Elements of complex capacitance matrix $\tilde{\mathsf{C}}$ and inductance matrix $\tilde{\mathsf{L}}$ for the structure of Fig. 7 at 10 GHz as a function of the substrate loss factor. (a) Entries of $\mathrm{Re}\,(\tilde{\mathsf{C}}) = \mathsf{C}$ compared to $-\mathrm{Im}(\tilde{\mathsf{C}}) = \mathsf{G}/\omega$ (scaled by a factor of 10 for clearness). (b) Elements of $\mathrm{Re}\,(\tilde{\mathsf{L}}) = \mathsf{L}$ compared to $-\mathrm{Im}(\tilde{\mathsf{L}}) = \mathsf{R}/\omega$.

which can be explained as follows. Each pair can roughly be approximated as a symmetric line pair in its own respect. For such a line, the two fundamental modes β_{even} and β_{odd} are found from

$$\begin{aligned}\beta_{\text{even}}^2 &= -(j\omega(C_s - |C_m|) + (G_s + G_m)) \\ &\quad \cdot (j\omega(L_s + L_m) + (R_s + R_m)) \\ \beta_{\text{odd}}^2 &= -(j\omega(C_s + |C_m|) + (G_s - G_m)) \\ &\quad \cdot (j\omega(L_s - L_m) + (R_s - R_m)) \end{aligned} \tag{55}$$

in which the indices s and m denote the diagonal, respectively, the off-diagonal elements from the (2×2) circuit matrices associated with each line pair. As an illustration, Fig. 10 shows the relevant elements of the complex matrices $\tilde{\mathsf{C}}$ and $\tilde{\mathsf{L}}$ associated with the conductor pair c_3–c_4. The elements C_{33} and C_{44} correspond to C_s from (55) (the small difference between them is due to the actual nonsymmetry of the configuration), whereas C_{34} corresponds to C_m. From Fig. 10(a), it becomes clear that the factor $(j\omega C_s + G_s)$ in (55) is dominated by the capacitance term and the numerical results confirm this is also the case for the other line pairs. For all line pairs, both C_s (positive) and C_m (negative) are influenced in the same way by the charge on the substrate's surface. As soon as the loss tangent becomes larger than approximately 1, an increasing σ_{sub} increases C_s, whereas $|C_m|$ decreases. For the odd mode, depending on $C_s + |C_m|$, the influence of σ_{sub} is cancelled out, whereas it is reinforced for the even mode. This explains the flat behavior of the SWF in Fig. 9(a) around $\sigma_{\text{sub}}/\omega\epsilon_{\text{sub}} \approx 1$ for the odd modes, and the increase for the even modes. This effect is not very pronounced for mode m_4, although an "even" mode. This is due to the reference conductor, shielding c_5 and c_6 from the substrate. The reason why m_3 has the highest and m_1 the lowest SWF from the even modes is readily explained as well. The influence of the reference conductor and the doped part (σ_{dop}) in the substrate lead to higher capacitance elements associated with the conductors on the left (c_1, c_2, c_5, and c_6, strongly excited in mode m_3) than for those on the right (excited in mode m_1). At higher values of σ_{sub}, when the magnetic field can no longer fully penetrate the substrate, an analog argumentation based on the inductance and resistance coefficients explains the different σ_{sub} dependence of the odd and even modes.

Fig. 9 also shows that the overall odd-mode SWF is higher than for the even modes. As both conductors of each pair are close to one another, $|C_m|$ is of the same order of magnitude as C_s, and $(C_s + |C_m|)$ is, hence, considerably larger than $(C_s - |C_m|)$. Furthermore, $|j\omega L_s + R_s|$ is considerably higher than $|j\omega L_m + R_m|$ due to the large line resistance R_m [see Fig. 10(b)]. Going back to (55), the above considerations immediately lead to the observed difference in magnitude of the SWF of the even and odd modes.

Similar reasonings can be put forward to explain the attenuation constants. The main effect here is that the odd modal currents, opposite in both conductors of each pair, tend to repel each other, and hence, flow through a smaller effective area of the conductors than the currents of the even modes, resulting in a higher attenuation.

The conductance coefficients G_{33}, G_{34}, and G_{44}, shown in Fig. 10(a), clearly demonstrate the semiconductor's behavior. For a very low conductivity σ_{sub}, $\mathbf{e}_t$ must be taken into account, but the transverse currents $\sigma_{\text{sub}}\mathbf{e}_t$ are still negligible.

Authorized licensed use limited to: AT & T. Downloaded on May 13, 2009 at 10:24 from IEEE Xplore. Restrictions apply.

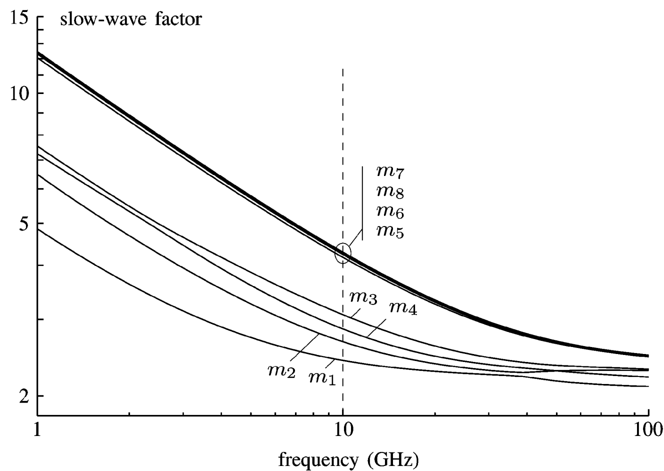

Fig. 11. SWF as a function of frequency for the fundamental modes from m_1 to m_8 of Fig. 7 (with $\sigma_{\rm sub} = 2$ S/m). The dotted line denotes the frequency at which the modal voltages are shown in Fig. 3.

When $\sigma_{\rm sub}$ increases, the transverse currents and the G values also increase. However, as soon as the loss tangent becomes considerably higher than 1, charge relaxation reduces $\mathbf{e}_t$. This effect outweighs the increase in $\sigma_{\rm sub}$, and hence, the G values decrease again, and in the end, become negligible as soon as the substrate's surface potential has become constant.

Finally, the frequency dependency of the SWF is shown in Fig. 11 for a substrate conductivity $\sigma_{\rm sub} = 2$ S/m. The transition from the *RC* to the *LC* range takes place around 20 GHz. This frequency is quite high because the conductors' cross sections are small, resulting in large R values.

VII. Conclusion

A new MTL model has been developed, which is valid for general 2-D lossy line configurations within the quasi-TM frequency range.

A careful theoretical analysis proves that within the quasi-TM limit, semiconductors can be accurately modeled by only considering two different regimes as a function of their loss factor. For highly doped semiconductors, the boundary potential becomes constant, and their longitudinal current is taken into account. Lowly doped semiconductors can be treated as lossy dielectrics. In the quasi-TM limit, these two regimes suffice to obtain accurate and continuous results as a function of conductivity and frequency.

We have also shown how an existing quasi-TM model for a single line can be extended to coupled lines. For this, a reciprocity-based approach as compared to a power-based one has proven to be necessary, leading to a nonconventional definition of the circuit modal currents (as compared to classical quasi-TEM models in the sole presence of low-loss dielectrics). To obtain the resistance, inductance, conductance, and capacitance (RLGC) circuit matrices, solving two boundary integral equations (one for the complex capacitance problem and one for the complex inductance problem) combined with the Dirichlet to Neumann boundary operator for the different materials, turned out to be sufficient.

A number of single conductor lines were simulated, showing excellent agreement with results already available in literature, and the possibilities of the method were further explored by considering an eight-line multiconductor example of an on-chip configuration.

References

[1] G. Plaza, R. Marques, and F. Medina, "Quasi-TM MoL/MoM approach for computing the transmission-line parameters of lossy lines," *IEEE Trans. Microw. Theory Tech.*, vol. 54, no. 1, pp. 198–209, Jan. 2006.

[2] E. Groteluschen, L. S. Dutta, and S. Zaage, "Quasi-analytical analysis of the broadband properties of multiconductor transmission lines on semiconducting substrates," *IEEE Trans. Compon., Packag., Manuf. Technol. B*, vol. 17, no. 3, pp. 376–382, Aug. 1994.

[3] H. Ymeri, B. Nauwelaers, K. Maex, and D. De Roest, "Influence of a lossy silicon substrate on conductance and capacitance of coupled interconnects," *J. Microw. Optoelectron.*, vol. 3, no. 3, pp. 49–53, Dec. 2003.

[4] U. Arz, H. Grabinski, and D. F. Williams, "Influence of the substrate resistivity on the broadband propagation characteristics of silicon transmission lines," in *54th ARFTG Conf. Dig.*, Dec. 1999, vol. 36, pp. 65–70.

[5] G. Manetas, V. N. Kourkoulos, and A. C. Cangellaris, "Investigation on the frequency range of validity of electroquasistatic *RC* models for semiconductor substrate coupling modeling," *IEEE Trans. Electromagn. Compat.*, vol. 49, no. 3, pp. 577–584, Aug. 2007.

[6] F. Bertazzi, G. Ghione, and M. Goano, "Efficient quasi-TEM frequency-dependent analysis of lossy multiconductor lines through a fast reduced-order FEM model," *IEEE Trans. Microw. Theory Tech.*, vol. 51, no. 9, pp. 2029–2035, Sep. 2003.

[7] F. Bertazzi, F. Cappelluti, S. Guerrieri, F. Bonani, and G. Ghione, "Self-consistent coupled carrier transport full-wave EM analysis of semiconductor traveling-wave devices," *IEEE Trans. Microw. Theory Tech.*, vol. 54, no. 4, pp. 1611–1618, Jun. 2006.

[8] J. Aguilera, R. Marques, and M. Horno, "Improved quasi-static spectral domain analysis of microstrip lines on high-conductivity insulator-semiconductor substrates," *IEEE Microw. Guided Wave Lett.*, vol. 9, no. 2, pp. 57–59, Feb. 1999.

[9] J. J. Kucera and R. J. Gutmann, "Effect of finite metallization and inhomogeneous dopings on slow-wave-mode propagation," *IEEE Trans. Microw. Theory Tech.*, vol. 45, no. 10, pp. 1807–1810, Oct. 1997.

[10] Y. R. Kwon, V. M. Hietala, and K. S. Champlin, "Quasi-TEM analysis of 'slow-wave' mode propagation on coplanar microstructure MIS transmission lines," *IEEE Trans. Microw. Theory Tech.*, vol. MTT-35, no. 6, pp. 545–551, Jun. 1987.

[11] F. Olyslager and D. De Zutter, "Rigorous boundary integral equation solution for general isotropic and uniaxial anisotropic dielectric waveguides in multilayered media including losses, gain and leakage," *IEEE Trans. Microw. Theory Tech.*, vol. 41, no. 8, pp. 1385–1392, Aug. 1993.

[12] F. Olyslager, *Electromagnetic Waveguides and Transmission Lines*. Oxford, U.K.: Oxford Univ. Press, 1999.

[13] F. Olyslager, D. de Zutter, and A. T. de Hoop, "New reciprocal circuit model for lossy waveguide structures based on the orthogonality of the eigenmodes," *IEEE Trans. Microw. Theory Tech.*, vol. 42, no. 12, pp. 2261–2269, Dec. 1994.

[14] L. Wiemer and R. H. Jansen, "Reciprocity related definition of strip characteristic impedance of multiconductor hybrid-mode transmission lines," *Microw. Opt. Technol. Lett.*, vol. 1, no. 1, pp. 22–25, Mar. 1988.

[15] G. Cano, F. Medina, and M. Horno, "Efficient spectral domain analysis of generalized multistrip lines in stratified media including thin, anisotropic, and lossy substrates," *IEEE Trans. Microw. Theory Tech.*, vol. 40, no. 2, pp. 217–227, Feb. 1992.

[16] F. Mesa, G. Cano, F. Medina, R. Marques, and M. Horno, "On the quasi-TEM and full-wave approaches applied to coplanar multistrip on lossy dielectric layered media," *IEEE Trans. Microw. Theory Tech.*, vol. 40, no. 3, pp. 524–531, Mar. 1992.

[17] D. De Zutter and L. Knockaert, "Skin effect modeling based on a differential surface admittance operator," *IEEE Trans. Microw. Theory Tech.*, vol. 53, no. 8, pp. 2526–2538, Aug. 2005.

[18] D. De Zutter, H. Rogier, L. Knockaert, and J. Sercu, "Surface current modelling of the skin effect for on-chip interconnections," *IEEE Trans. Compon., Packag., Manuf. Technol. B*, vol. 30, no. 2, pp. 342–349, May 2007.

[19] K. Wu and R. Vahldieck, "Hybrid-mode analysis of homogeneously and inhomogeneously doped low-loss slow-wave coplanar transmission lines," *IEEE Trans. Microw. Theory Tech.*, vol. 39, no. 8, pp. 1348–1360, Aug. 1991.

Authorized licensed use limited to: AT & T. Downloaded on May 13, 2009 at 10:24 from IEEE Xplore. Restrictions apply.

Thomas Demeester was born in Ghent, Belgium, in 1982. He received the M.Sc. degree in electrical engineering from Ghent University, Ghent, Belgium, in 2005, and is currently working toward the Ph.D. degree at Ghent University.

He spent one year with ETH Zürich, where he was involved in the field of time-domain electromagnetics. He is a Research Fellow of the Fund for Scientific Research (FWO-V), Flanders, Belgium. His research concerns electromagnetic field calculations in the presence of highly lossy media and the development of transmission line models for interconnects.

Daniël De Zutter (M'92–SM'96–F'01) was born in 1953. He received the M.Sc. degree in electrical engineering, Ph.D. degree, and a thesis leading to a degree equivalent to the French Aggrégation or the German Habilitation from Ghent University, Ghent, Belgium, in 1976, 1981, and 1984, respectively.

From 1984 to 1996, he was with the National Fund for Scientific Research of Belgium. He is currently a Full Professor of electromagnetics with Ghent University. Most of his earlier scientific work concerned the electrodynamics of moving media. His research currently focuses on all aspects of circuit and EM modeling of high-speed and high-frequency interconnections and packaging, EM compatibility, and numerical solutions of Maxwell's equations. He has authored or coauthored over 140 international journal papers and 150 papers in conference proceedings.

Prof. De Zutter is an associate editor for the IEEE TRANSACTIONS ON MICROWAVE THEORY AND TECHNIQUES. He was a corecipient of the 1995 IEEE Microwave Prize Award presented by the IEEE Microwave Theory and Techniques Society (IEEE MTT-S). He was the recipient of the 1999 Transactions Prize Paper Award presented by the IEEE Electromagnetic Compatibility (EMC) Society.

Authorized licensed use limited to: AT & T. Downloaded on May 13, 2009 at 10:24 from IEEE Xplore. Restrictions apply.